RFI DETECTION AND MITIGATION USING INDEPENDENT COMPONENT ANALYSIS AS A PRE-PROCESSOR

Adam J. Schoenwald [1,2,3] *, Armen Gholian*[1]*, Damon C. Bradley* [1]*, Mark Wong* [1]*,*
Priscilla N. Mohammed [1,4]*, Jeffrey R. Piepmeier* [1]

(1) NASA Goddard Space Flight Center, Greenbelt, MD
(2) ASRC Federal Space and Defence, Greenbelt, MD
(3) University of Maryland, Baltimore County
(4) Goddard Earth Sciences Technology and Research, Morgan State University

ABSTRACT

Radio-frequency interference (RFI) has negatively impacted scientific measurements of passive remote sensing satellites. This has been observed in the L-band radiometers Soil Moisture and Ocean Salinity (SMOS), Aquarius and more recently, Soil Moisture Active Passive (SMAP). RFI has also been observed at higher frequencies such as K band. Improvements in technology have allowed wider bandwidth digital back ends for passive microwave radiometry. A complex signal kurtosis radio frequency interference detector was developed to help identify corrupted measurements. This work explores the use of Independent Component Analysis (ICA) as a blind source separation (BSS) technique to pre-process radiometric signals for use with the previously developed real and complex signal kurtosis detectors.

Index Terms— Interference, Circularity, Complex Random Process, Radiometer, Digital Receiver, Kurtosis, Complex Kurtosis, Independent Component Analysis

1. INTRODUCTION

As the radio spectrum becomes saturated, microwave radiometry remote sensing instruments must deal with both shared spectrum as well unintentionally contaminated spectrum. Recent advances in high speed radio frequency (RF) electronics has enabled wideband remote sensing techniques while simultaneously allowing for a more crowded spectrum. To help identify a corrupted measurement, a real time radio frequency interference (RFI) detection algorithm can be used in a radiometer digital back end such as the one used on the radiometer for the Soil Moisture Active Passive (SMAP) mission [1].

While higher order test statistics prove effective at detecting pulsed interference [2], it is more difficult to detect continuous interference and complex modulations using the same statistical methods. To this end additional test statistics in previous work [3, 4, 5] were evaluated. This work now applies Independent Component Analysis (ICA) as a pre-processor for RFI detection.

Thanks to NASA Earth Science Technology Office NNH13ZDA001N ACT Funding

2. HYPOTHESIS TESTING

With the goal of developing new RFI detection algorithms and evaluating their performance, hypothesis testing is used. The signal is modeled under null and alternate hypothesis. For the null hypothesis, H_0 , it is assumed that the radiometer only observes thermal noise. Under the alternate hypothesis, H_1 , the radiometer observes both thermal noise as well as a source of interference.

$$H_0 : \textit{Thermal Noise Only}$$
$$H_1 : \textit{Thermal Noise and Interference}$$

The primary goal of this work is to increase the ability to differentiate between H_0 and H_1. A secondary goal of this work is to obtain the ability to determine what the measurement would have been if the interference did contaminate the observation.

2.1. Signal Model

In the context of microwave radiometry remote sensing, it is assumed that the the receiver consists of a single dual polarization antenna. This gives instantaneous access to observations of the horizontal and vertical polarizations, $x_H(t)$ and $x_V(t)$. The geophysical thermal noise is considered to be a Gaussian random process, with the horizontal (1) and vertical (2) polarizations being uncorrelated and independent (3).

$$W_H(t) \sim \mathcal{N}(0, \sigma_n^2) \tag{1}$$

$$W_V(t) \sim \mathcal{N}(0, \sigma_n^2) \tag{2}$$

$$W_H(t) \perp W_V(t) \tag{3}$$

To accurately capture the nature of satellite communications it is assumed that the interfering signal, $r(t)$ is circularly polarized, resulting in a 90 degree phase shift between the two channels, $r_H(t)$ and $r_V(t)$ as shown in equation (4). The variance of the interfering signal is denoted by σ_r^2 , and assumed to be equal in both polarizations.

$$r_H(t) = r_V(t)e^{\frac{-j\pi}{2}} \tag{4}$$

This leads us to a more accurate definition of the two hypothesis cases shown in equation (5).

$$\begin{aligned} H_0 &: \begin{cases} x_H(t) &= W_H(t) \\ x_V(t) &= W_V(t) \end{cases} \\ H_1 &: \begin{cases} x_H(t) &= W_H(t) + r_H(t) \\ x_V(t) &= W_V(t) + r_V(t) \end{cases} \end{aligned} \tag{5}$$

The interference to noise ratio (INR) is defined as the ratio between the interference variance, σ_r^2, and noise variance, σ_n^2, as expressed in decibels by equation (6).

$$\mathrm{INR}_{\mathrm{dB}} = 10\log_{10}\frac{\sigma_r^2}{\sigma_n^2} \tag{6}$$

By varying the INR and running Monte-Carlo simulations, the efficacy of different test statistics and detection schemes can be evaluated.

2.2. Real Signal Kurtosis

Real signal kurtosis (RSK) [2] is used as a test statistic that is well suited toward both real and complex signals. Given a complex baseband signal $z(n) = I(n) + jQ(n)$, the fourth standardized moment is computed independently for both the real and imaginary vectors, I and Q as was used on SMAP [1].

$$\mathrm{RSK}_I = \frac{\mathbb{E}\left[(I - \mathbb{E}[I])^4\right]}{\mathbb{E}\left[(I - \mathbb{E}[I])^2\right]} - 3 \tag{7}$$

$$\mathrm{RSK}_Q = \frac{\mathbb{E}\left[(Q - \mathbb{E}[Q])^4\right]}{\mathbb{E}\left[(Q - \mathbb{E}[Q])^2\right]} - 3 \tag{8}$$

The test statistic, RSK, is then defined in equation (9) as

$$\mathrm{RSK} = \frac{|\mathrm{RSK}_I| + |\mathrm{RSK}_Q|}{2} \tag{9}$$

As the RSK test statistic deviates from zero, signal is considered to be less Gaussian and more likely to contain interference.

2.3. Complex Signal Kurtosis

Given a complex baseband signal $z(n) = I(n) + jQ(n)$, moments $\alpha_{\ell,m}$ are defined in equation (10).

$$\alpha_{\ell,m} = \mathbb{E}\left[(z - \mathbb{E}[z])^{\ell}(z - \mathbb{E}[z])^{*m}\right], \quad \ell, m \in \mathbb{N}_{\geq 0} \tag{10}$$

With $\sigma^2 = \alpha_{1,1}$, Standardized moments $\varrho_{\ell,m}$ can be found as shown in equation (11).

$$\varrho_{\ell,m} = \frac{\alpha_{\ell,m}}{\sigma^{\ell+m}}, \tag{11}$$

This leads to the CSK (Complex Signal Kurtosis) RFI Test statistic [3, 4, 5] as shown in equation (12).

$$CSK = \frac{\varrho_{2,2} - 2 - |\varrho_{2,0}|^2}{1 + \frac{1}{2}|\varrho_{2,0}|^2} \tag{12}$$

Similarly to the RSK test statistic, as CSK deviates from zero it is considered to be more likely to contain interference.

3. INDEPENDENT COMPONENT ANALYSIS PRE-PROCESSOR

In an effort to both identify interference as well as remove it from measurements, the blind source separation (BSS) method ICA was used in this work as a pre-processing algorithm.

3.1. Independent Component Analysis

ICA assumes that originating sampled sources, $\mathbf{s(n)} = (s_1(n), \ldots, s_M(n))^T$, are mixed by an instantaneous constant mixing matrix $\mathbf{A}$, into an observable $\mathbf{x(n)} = (x_1(n), \ldots, x_M(n))^T$ as shown in (13). The use of a de-mixing matrix $\mathbf{W}$ is used to invert the mixing process and retrieve the original signal. Since access to true values of $\mathbf{s}$ and $\mathbf{W}$ are unavailable, they are estimated as shown in (14) by iteratively modifying $\hat{\mathbf{W}}$ and checking if $\hat{\mathbf{s}}$ meets a separation criteria. This iterative process is roughly illustrated in Figure 1.

$$\mathbf{x(n)} = \mathbf{As(n)} \tag{13}$$

$$\hat{\mathbf{s}} = \hat{\mathbf{W}}\mathbf{x} \tag{14}$$

3.2. ICA Preprocessor Implementation

ICA was used as a pre-processor to the existing test statistics RSK (9) and CSK (12). The separation of the observed signal into its underlying components is an attempt to increase the sensitivity of the detector. Test statistics are then taken on the estimated original signals, $\hat{\mathbf{s}}$ instead of the observed signals in $\mathbf{x}$ as seen for the RSK case in Figure 2.

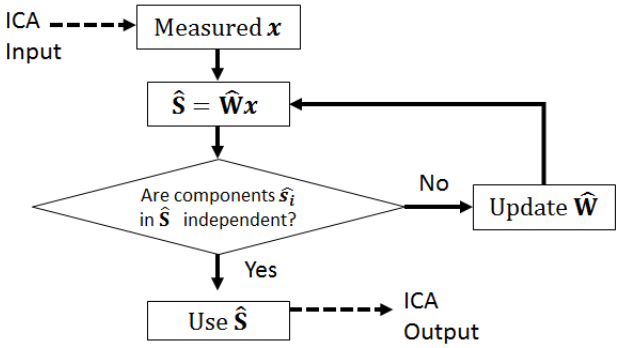

Fig. 1. Flow chart showing top level view of ICA.

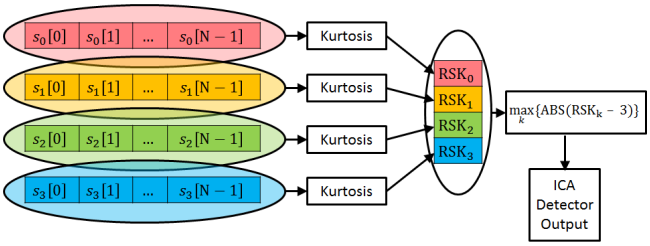

Fig. 2. Block diagram depicting how the output of ICA is used as pre-processed data for RSK.

3.3. ICA RFI Excision

In addition to RFI detection, once identified one could use the existing information to determine what would have been observed had the interference not been present. By replacing an entire row in $\hat{\mathbf{s}}$ with zeros and coming back through the inverse of $\hat{\mathbf{W}}$. The new filtered set of estimated signals with zeroed out interference components is denoted by $\tilde{\mathbf{s}}$. Denoting the inverse of $\hat{\mathbf{W}}$ as $\hat{\mathbf{A}}$, an estimated RFI free observation $\tilde{\mathbf{x}}$ is obtained as shown in (15).

$$\tilde{\mathbf{x}} = \hat{\mathbf{A}}\tilde{\mathbf{s}} \tag{15}$$

If the only desired parameter of $\tilde{\mathbf{x}}$ is the variance of each vector, $\tilde{\mathbf{x}}$ need not be computed. The variance of each vector in $\hat{\mathbf{s}}$ is normalized to one and the variances of $\tilde{\mathbf{x}}$ lie in the non RFI associated coefficients of the $\hat{\mathbf{A}}$ matrix.

3.4. ICA Algorithms Used

An assortment of different ICA algorithms were tested as enumerated below. The algorithms differ in their use of real and complex valued values, as well as the sources of diversity and statistical assumptions used to identify the de-mixing matrix.

- Fast ICA (FASTICA) [6, 7]
- Robust ICA (ROBUSTICA) [8, 9]
- Non Circular Complex Fast ICA (NCCFASTICA) [10, 11]
- Entropy Rate Bound Minimization (ERBM) [12, 11]
- Complex Quadrature Amplitude Modulation (CQAM-SYM) [13, 11]
- Complex Entropy Rate Bound Minimization (CERBM) [14, 11]

4. RESULTS

Monte-Carlo simulations were run at varying values of INR to evaluate the performance of the different ICA algorithm and detector combinations. For every simulation, 9000 samples were collected before performing any ICA pre-processing or computing test statistics. A receiver operating characteristic (ROC) curve was computed for every set of parameters, and the area under the curve (AUC) was used as figure of merit. As AUC approaches 1 the detector is performing at its best, while as it approaches 0.5 the detector is not able to differentiate between the two cases. By looking at the INR when the AUC crosses 0.75, a single numerical performance value with which to compare multiple detection algorithms is obtained. The simulations were run using pulsed continuous wave (PCW), continuous wave (CW), and quadrature phase shift keying (QPSK) forms of interference.

4.1. Results for PCW Modulation

When differentiating between the two hypothesis while considering pulsed continuous wave modulation the combination of robust ICA with RSK performed best as shown in Figure 3.

4.2. Results for CW Modulation

While using a continuous wave modulation the CERBM algorithm provides the largest gain in interference detectability as shown in Figure 4. This may be due to the fact that CERBM uses sample to sample dependence in addition to higher order statistics when finding the de-mixing matrix. A non-pulsed signal should provide consistent sample to sample dependence across the entire duration of the observation.

4.3. Results for QPSK Modulation

While using a wideband (QPSK) modulation the CERBM algorithm once again provides the largest gain in interference detectability as shown in Figure 5. The QPSK signal evaluated here occupies 15% of the digital bandwidth, and is convolved with a Root-raised-cosine (RRC) filter similar to those used for single carrier satellite communications.

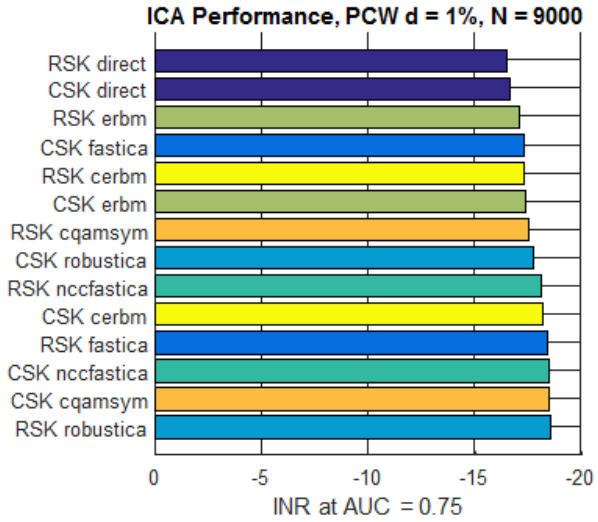

Fig. 3. Detector performance when using a pulsed continuous wave interferer.

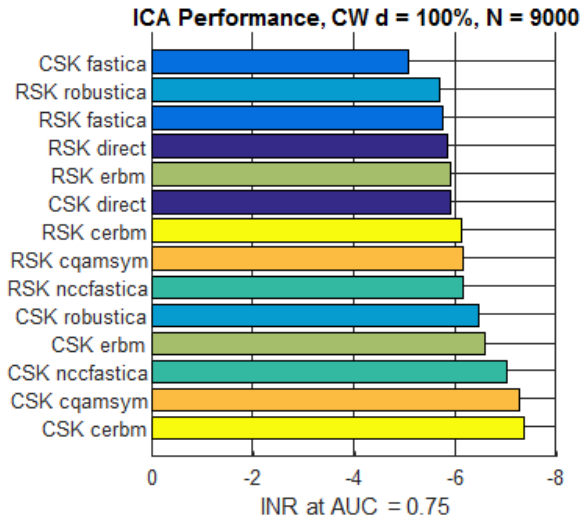

Fig. 4. Detector performance when using a continuous wave interferer.

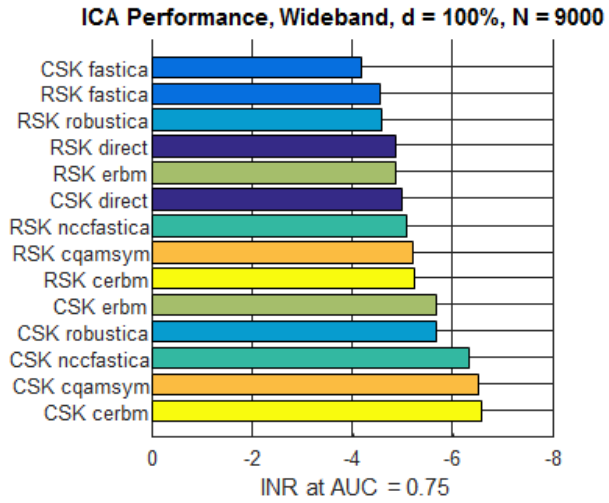

Fig. 5. Detector performance when using a pulsed wideband (QPSK) interferer.

5. CONCLUSIONS

From the results it is clear that some improvement can be made when using ICA as a pre-processor for RSK and CSK test statistics while trying to differentiate between clean thermal noise compared to an RFI corrupted observation. The performance boost in this work is limited to an increase of RFI detectability at about 2dB INR. This is likely due to the under determined nature of the available observations and mixing process. While the 2dB boost in detectable RFI levels may be beneficial, a significant improvement is still needed to mitigate the effects of continuous and complex interference on microwave radiometry instruments.

It would not be surprising to see a large gain in performance by increasing the number of observations, but this work is focused on the single dual polarization antenna case that is most applicable for remote sensing via space born satellite microwave radiometry.

To develop a multiple antenna system and increase the number of observations, the assumption of a instantaneous mixing matrix implies that the observations must be synchronized and be observing the same terrestrial footprint. This approach could also be used for RFI mitigation purposes with other system architectures where a larger number of observations are present.

6. REFERENCES

[1] J. R. Piepmeier, J. T. Johnson, P. N. Mohammed, D. Bradley, C. Ruf, M. Aksoy, R. Garcia, D. Hudson, L. Miles, and M. Wong, "Radio-frequency interference mitigation for the soil moisture active passive mi-

crowave radiometer," *IEEE Transactions on Geoscience and Remote Sensing*, vol. 52, no. 1, pp. 761–775, Jan 2014.

[2] R. D. De Roo, S. Misra, and C. S. Ruf, "Sensitivity of the kurtosis statistic as a detector of pulsed sinusoidal rfi," *IEEE Transactions on Geoscience and Remote Sensing*, vol. 45, no. 7, pp. 1938–1946, July 2007.

[3] D. Bradley, J. M. Morris, T. Adali, J. T. Johnson, and M. Aksoy, "On the detection of rfi using the complex signal kurtosis in microwave radiometry," in *Proc. 13th Specialist Meeting Microwave Radiometry and Remote Sensing of the Environment (MicroRad)*, Mar. 2014, pp. 33–38.

[4] D. C. Bradley, A. J. Schoenwald, M. Wong, P. N. Mohammed, and J. R. Piepmeier, "Wideband digital signal processing test-bed for radiometric rfi mitigation," in *2015 IEEE International Geoscience and Remote Sensing Symposium (IGARSS)*, July 2015, pp. 3489–3492.

[5] A. J. Schoenwald, D. C. Bradley, P. N. Mohammed, J. R. Piepmeier, and M. Wong, "Performance analysis of a hardware implemented complex signal kurtosis radio-frequency interference detector," in *Proc. 14th Specialist Meeting Microwave Radiometry and Remote Sensing of the Environment (MicroRad)*, Apr. 2016, pp. 71–75.

[6] A. Hyvarinen, "Fast and robust fixed-point algorithms for independent component analysis," *IEEE Transactions on Neural Networks*, vol. 10, no. 3, pp. 626–634, May 1999.

[7] ICA and Aalto University BSS Group, "Matlab resources," `http://research.ics.aalto.fi/ica/fastica/`.

[8] V. Zarzoso and P. Comon, "Robust independent component analysis by iterative maximization of the kurtosis contrast with algebraic optimal step size," *IEEE Transactions on Neural Networks*, vol. 21, no. 2, pp. 248–261, Feb. 2010.

[9] Institut Universitaire de France Vicente Zarzoso, "Robustica matlab resources," `http://www.i3s.unice.fr/~zarzoso/robustica.html`.

[10] M. Novey and T. Adali, "On extending the complex fastica algorithm to noncircular sources," *IEEE Transactions on Signal Processing*, vol. 56, no. 5, pp. 2148–2154, May 2008.

[11] University of Maryland Baltimore County Machine Learning for Signal Processing Laboratory, "Matlab resources," `http://mlsp.umbc.edu/resources.html`.

[12] X. L. Li and T. Adali, "Blind spatiotemporal separation of second and/or higher-order correlated sources by entropy rate minimization," in *Proc. Speech and Signal Processing 2010 IEEE Int. Conf. Acoustics*, Mar. 2010, pp. 1934–1937.

[13] M. Novey and T. Adalt, "Complex fixed-point ICA algorithm for separation of QAM sources using gaussian mixture model," in *Proc. IEEE Int. Conf. Acoustics Speech and Signal Processing - ICASSP '07*, Apr. 2007, vol. 2, pp. II–445–II–448.

[14] G. S. Fu, R. Phlypo, M. Anderson, and T. Adalı, "Complex independent component analysis using three types of diversity: Non-gaussianity, nonwhiteness, and noncircularity," *IEEE Transactions on Signal Processing*, vol. 63, no. 3, pp. 794–805, Feb. 2015.